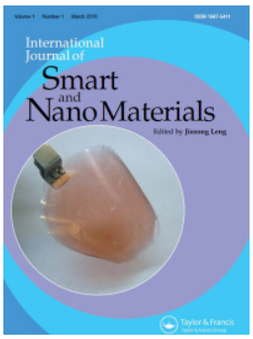

International Journal of Smart and Nano Materials

ISSN: (Print) (Online) Journal homepage: www.tandfonline.com/journals/tsnm20

Pinewood biochar antistatic polymer composites: an investigation of electrical, mechanical, rheological and thermal properties

Justin George, Sergejs Gaidukovs & Debes Bhattacharyya

To cite this article: Justin George, Sergejs Gaidukovs & Debes Bhattacharyya (26 Sep 2024): Pinewood biochar antistatic polymer composites: an investigation of electrical, mechanical, rheological and thermal properties, International Journal of Smart and Nano Materials, DOI: 10.1080/19475411.2024.2408013

To link to this article: https://doi.org/10.1080/19475411.2024.2408013

Published online: 26 Sep 2024.

INTERNATIONAL JOURNAL OF SMART AND NANO MATERIALS
https://doi.org/10.1080/19475411.2024.2408013

Taylor & Francis
Taylor & Francis Group

Pinewood biochar antistatic polymer composites: an investigation of electrical, mechanical, rheological and thermal properties

Justin George[a,b], Sergejs Gaidukovs[c] and Debes Bhattacharyya[a]

[a]Centre for Advanced Materials Manufacturing and Design, Faculty of Engineering, The University of Auckland, Auckland, New Zealand; [b]Carbon Research Centre, Carbon Dot Limited, Auckland, New Zealand; [c]Institute of Polymer Materials, Faculty of Materials Science and Applied Chemistry, Riga Technical University, Riga, Latvia

ABSTRACT

This study investigates the practical applications of biochar as an innovative and sustainable conductive filler in composite materials. Utilizing the conventional melt-blending method, we prepared conductive pinewood biochar-filled poly(lactic acid)/poly(butylene adipate-*co*-terephthalate) (PLA/PBAT) composites and systematically examined their electrical, mechanical, rheological and thermal properties. Our results reveal a significant enhancement of electrical and mechanical properties upon the inclusion of conductive pinewood biochar in the PLA/PBAT matrix. With the addition of 10 wt% of conductive pinewood biochar, the average surface resistivity of the composites decreased by three orders of magnitude, measuring $4.86 \times 10^{10}\Omega/\text{sq}$, which meets the antistatic requirements for polymer composites. Additionally, the average tensile strength of the biochar filler composites improved by 53% with an addition of just 1 wt% of biochar.

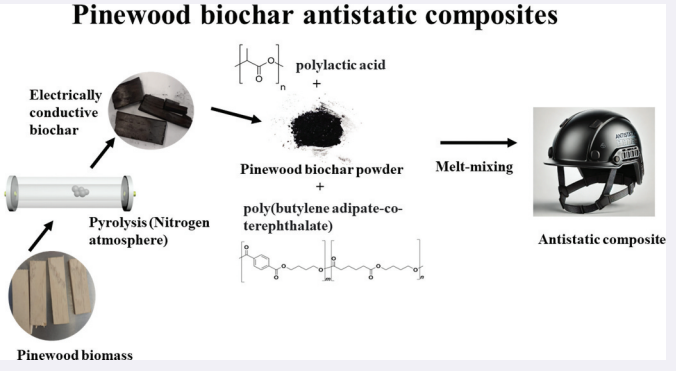

ARTICLE HISTORY
Received 10 July 2024
Accepted 17 September 2024

KEYWORDS
Biochar; pyrolysis; melt-blending; polymer composites; antistatic

CONTACT Justin George jgeo541@aucklanduni.ac.nz Centre for Advanced Materials Manufacturing and Design, Faculty of Engineering, The University of Auckland, 314-319 Khyber Pass Road, Newmarket, Auckland 1142, New Zealand

1. Introduction

The global need for antistatic and electrostatic dissipative (ESD) materials utilized in electronic packaging and personal protective equipment (PPE) for hazardous environments is on the rise [1,2]. Materials characterized by surface resistivity within the range of 1×10^5 to $1 \times 10^{12}\Omega/\text{sq}$ are classified as antistatic. Polymer composites exhibiting electrical conductivity with this range find applications in antistatic scenarios. Among various conductive fillers employed to improve electrical properties, carbon-based fillers offer additional benefits, including corrosion resistance, tuneable electrical and mechanical properties, high thermal stability, biocompatibility and ultraviolet radiation resistance [3–7].

Carbon-based fillers are extensively utilized in the polymer industry to improve both the mechanical and electrical properties of the polymer matrix. Graphene, carbon nanotubes (CNT), carbon black, carbon fiber and graphite are the most commonly employed conductive and reinforcing fillers in polymers [8,9]. However, these fillers are predominantly derived from nonrenewable sources, and their production processes often lack environmental friendliness [10]. In an endeavor to promote the utilization of carbon derived from biowaste, eco-friendly biochar produced from agricultural waste has emerged as a novel reinforcement filler. Biochar offers several advantages over conventional carbon-based fillers, including sustainability, renewability and cost-effectiveness [11–13]. However, the electrical conductivity of conventional biochar remains relatively low, with the highest reported value for monolithic biochar being 4.3 S/cm [14]. Therefore, achieving the desired electrical conductivity for the biochar polymer composites in the range of commercially accepted standard antistatic material proves challenging.

Although biochar proved to be an effective reinforcing filler in numerous polymers, its application as a conductive filler for antistatic and electrostatic dissipation materials is limited due to its low electrical conductivity. However, the characteristics of biochar can be tailored by adjusting the pyrolysis conditions and utilizing specific precursors. For instance, biochar synthesized at high temperatures in an inert atmosphere exhibits a high concentration of sp^2 carbon, which imparts electrical conductivity to the material [15]. Considering these tunable properties, biochar with a hierarchical porous structure, large surface area and high concentration of sp^2carbon can potentially be material for antistatic and electrostatic dissipation polymer composites.

Pinewood (*Pinus radiata*) waste, abundant in many countries, such as New Zealand, is an environmentally friendly and sustainable alternative reinforcing filler for polymer composites. Pinewood is widely utilized in manufacturing furniture and support structures due to its lightweight nature, dimensional stability, uniform grain and hierarchical structure [16]. Typically, pinewood waste, in the form of pinewood chips, finds application as animal bedding, building material, and bioenergy production [17]. The disposal of agricultural biomass waste into land and waterbodies contributes significantly to greenhouse gas emissions [18]. However, this agricultural biomass waste can be converted to value-added electrically conductive biochar with peculiar properties, such as large surface area, porous structure and highly stable carbon content, making it an attractive material for energy (electrode material) and manufacturing (reinforced conductive polymer composites) sectors [19–23].

This study introduces a chemical-free approach to biochar production by employing pinewood waste through pyrolysis at 1200 in an inert atmosphere. The resulting pinewood biochar exhibits enhanced growth of sp^2 carbon structures, contributing to an improvement in electrical conductivity. The resulting pinewood biochar was subsequently ground and sieved to a size less than 74 μm, and underwent comprehensive studies to gain insight into the structure, surface morphology, elemental content and functional group attached to the biochar through various techniques.

Pinewood biochar powder is integrated into biodegradable polymers like PLA and PBAT through melt-mixing, forming PLA/PBAT biochar composites. This study evaluates the mechanical, thermal, electrical and rheological properties and microstructure characteristics of these composites. This investigation aims to provide a comprehensive understanding of the potential antistatic applications of these biochar composites.

Although this research is primarily driven by the suitability of electrically conductive pinewood biochar for fabricating antistatic polymer composites, the study also aims at enhancing the mechanical and electrical properties, and the thermal conductivity values of these composites. This work serves the boarder purpose of creating innovative, eco-friendly antistatic material from pinewood biowaste.

The introduction of conductive pinewood biochar plays a crucial role in improving the compatibility between PLA and PBAT and, consequently, enhancing the mechanical properties of the composites. Notably, both the electrical and mechanical properties of the PLA-based composites surpass those reported in previous studies on PLA-based biochar composites [24,25]. These composites offer tuneable properties and provide valuable insights for the development of sustainable and high-performance materials for various applications.

2. Materials and methods

NatureWorks LLC, U.S.A., supplied 3D printing grade poly(lactic acid) (PLA), known as Ingeo BioPolymer 3D850. The PLA was in the pellet form with a specific density of 1.24 g/cm^3 and a melt flow rate of 7–9 g/10 min (ASTM D1238). Clariant, New Zealand, supplied poly(butylene adipate-*co*-terephthalate) (PBAT) pellets. Specific product details include the item as Renol 03459 PBAT CMP Natural. The PBAT had a 1.27 g/ml density at 20°*C* as per ISO 1183–1 and a melt flow index (MFI) (190°*C*; 2.16 kg) of 4 g/10 min (ASTM D1238).

2.1. Preparation of pinewood waste biochar

Pinewood biochar was produced through pyrolysis of pinewood chips (supplied by Bunnings Warehouse, Auckland, New Zealand) at 1200 in an inert gas at a heating ramp of 10/min and kept at 1200 for 60 min using a high-temperature tube furnace (SAF therm, Model: STG-100-17, China) and cooled to 700°*C* at a cooling rate of 5/min and then down to room temperature by natural cooling. The pinewood biochar was ground to powder and sieved using 200-mesh to under 74μm diameter and stored in a desiccator. The biochar powder was further characterized using SEM-EDS, Raman spectroscopy and XPS.

Table 1. Nomenclatures of the polymer composites.

Composites	PLA (wt%)	PBAT (wt%)	PWBC (wt%)
PLA (80/20)	80	20	0
PLA (79/20/1)	79	20	1
PLA (77.5/20/2.5)	77.5	20	2.5
PLA (75/20/5)	75	20	5
PLA (70/20/10)	70	20	10

2.2. Preparation of pinewood biochar composites

Different formulations of PLA (70, 75, 77.5, 79 and 80 wt%), PBAT (20 wt%) and biochar (BC) (0, 1, 2.5, 5 and 10 wt%) were melt-mixed (Table 1) to obtain PLA/PBAT/pinewood biochar (PWBC) composites using a Brabender mixer (Plasti-Corder Lab-station) at mixing temperature (200),a screw rotation speed of 70 rpm/min for a mixing time of 5 min.

Pinewood biochar powder, poly(lactic acid) and PBAT were dried at 80 for 1440 min to remove moister content and were weighed and premixed before melt-mixing. The mixture is then introduced into 50cm^3 mixing chamber, which was maintained at the set condition mentioned earlier. After the specified mixing time, the composites were collected and pelletized by a pelletizing mill (Model: IZ-120, Lab tech Engineering Company Ltd, Thailand) before injection molding. The pellets were dried at a temperature of at 72°C for 1440 min, compression molded to thin sheets of (100 mm × 100 mm × 5 mm) size, and used for the electrical studies. The tensile testing samples were injection molded using injection molding machine from Dr Boy, Neustadt, Germany.

2.3. Characterisations of pinewood biochar and composites

The scanning electron microscope Hitachi SU-70 FE-SEM was employed to examine the surface morphology of fractured surfaces of tensile samples. In order to prevent charging and enhance secondary electron emission, all samples underwent platinum coating. The secondary electron SEM utilizes a low acceleration voltage of 5kV.

The transmission electron microscope (FEI Tecnai FEG20), equipped with a field emission gun and operated at an acceleration voltage of 200 kV, was used to capture HRTEM images. ImageJ software was then used to perform fast Fourier transform (FFT) analysis on the HRTEM images.

Raman spectroscopy studies were conducted using a LabRAM HR evolution confocal Raman microscope. Biochar powder samples (prepared with mortar and pestle) were used for Raman studies to ensure sample homogeneity. A 532 nm laser line, and a 50× objective lens was employed to collect all Raman data.

X-ray photoelectron spectroscopy (XPS) analysis was conducted using a Kratos Axis DLD XPS system with high energy resolution discussed elsewhere [25]. FEI Tecnai FEG 20, with an acceleration voltage of 200 kV TEM equipped with a field emission electron source, was used to image a high-resolution graphitic lattice in biochar.

The differential scanning calorimetry (DSC) study was conducted using the DSC Q 1000 instrument from TA instruments in New Castle, DE, U.S.A. The temperature profile was from 30 to 200 °*C*, and cooling was from 200 to 30 °*C* at a rate of 10 °*C*/min, and hold time of 1 min; the samples were then heated again to 200 °*C*,

before being tested using a heat-cool-heat cycle as discussed in the previous study [25]. The calculations of the composites' crystallinity are discussed elsewhere [26–28].

Thermogravimetric analysis (TGA) was performed on the composite samples using the TGA Q 5000 from TA instruments in New Castle, DE, U.S.A. The temperature profile used in the analysis was discussed elsewhere [25].

Mechanical properties were studied using an Instron 5567 universal tensile testing machine (Norwood, MA, U.S.A.) according to ASTM D638 protocol. Type IV compression molded samples were used for the studies. Electrical studies on four samples from each set were carried out using Keithly resistive meter 6517A (supplied by ValueTronics International, Inc, Illinois, U.S.A.) according to ASTM D257.

The rheological behavior of the composites was examined with an Anton Paar SmartPave 102 rheometer (Graz, Austria) in a 25 mm plate–plate configuration through oscillatory shear tests at temperature of 195 $^{\circ}C$ for the composites. The complex viscosity was assessed over a shear range spanning from 0.1 to 628 rad/s, maintaining a constant shear strain amplitude of 5%. The rheometer temperature was maintained at 175 for PLA (80/20) and 195 for the other samples.

Thermal conductivity was studied using a light flash apparatus (LFA) Netzsch 447 NanoFlash (NETZSCH-Geratebau GmBH, SelB, Germany) according to EN ISO 22,007–4. The heat capacity of the samples was obtained compared to a Pyrex sample with a known heat capacity. The details of thermal conductivity studies are discussed elsewhere [29].

3. Results and discussion

3.1. Biochar characterisation

The pinewood biomass was converted to biochar with a hierarchical structure, Figure 1, through pyrolysis. To enhance the dispersion of biochar within the polymer, pinewood biochar blocks were ground and sieved into particles smaller than 74 μ size before being mixed with the polymer matrix through melt-mixing. The particle lengths ranged from 2.5 to 70 μ with a mean value of 11.5 μ and a standard deviation of 14.7 μ. This procedure was crucial in achieving a consistent distribution of biochar throughout the polymer matrix, thereby improving the electrical and mechanical characteristics of the composite material.

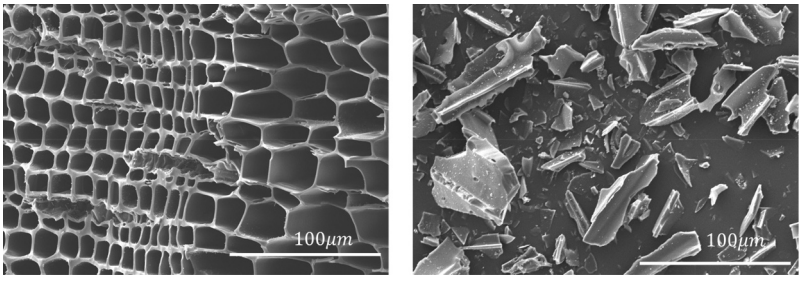

Figure 1. SEM images of (a) pinewood biochar and (b) pinewood biochar powder.

3.2. Raman spectroscopy of pinewood biochar

Figure 2 displays the Raman spectrum of pinewood biochar (*p*-1200), depicting characteristic peaks at 1345 cm^{-1} corresponding to the D band and 1601 cm^{-1} corresponding to the G band. The deconvolution process for the D and G bands of pinewood biochar was executed, resulting in the fitting of a total of four peaks, as illustrated in Figure 3. The G mode of the vibrational band is linked to the in-plane vibration of sp^2 carbon atoms. In contrast, the D band arises from the breathing mode of aromatic rings, as shown in the schematic diagram of Figure 2 inset. In perfect crystalline graphite, the D band is absent but characterized by a sharp G band; however, the D band is prevalent for defective graphene and other sp2 carbon (carbon black, biochar and carbon nanotubes). The broadened G and D bands have additional peaks fit at ~1180$cm^{-1}$and ~1530cm^{-1}, which are D^* and D^{**} respectively. Ferrari and Robertson have shown that these peaks are the sum and differences of C = C stretching and CH wagging modes (sp^2 carbon) rather than from sp^3 hybridised carbon [30]. These two peaks have previously been observed in nanocrystalline graphite produced through ball milling [30]. These findings indicate that these peaks are neither from remnant functional groups nor from sp^3 hybridised carbon, instead, exist due to finite-size graphitic crystallites and defects originating during pyrolysis and size reduction [31]. The ratio of D and G band intensities (I_D/I_G) indicates the defects associated with the biochar. For the pinewood biochar, the $I_D/I_G = 2.9$, which indicates that the biochar has high defect concentration. Although I_D/I_G ratio is attributed to the defect density associated with the graphitic structures; some authors have mentioned that D band intensity depends on graphitic crystal size [32]. However, recent studies have

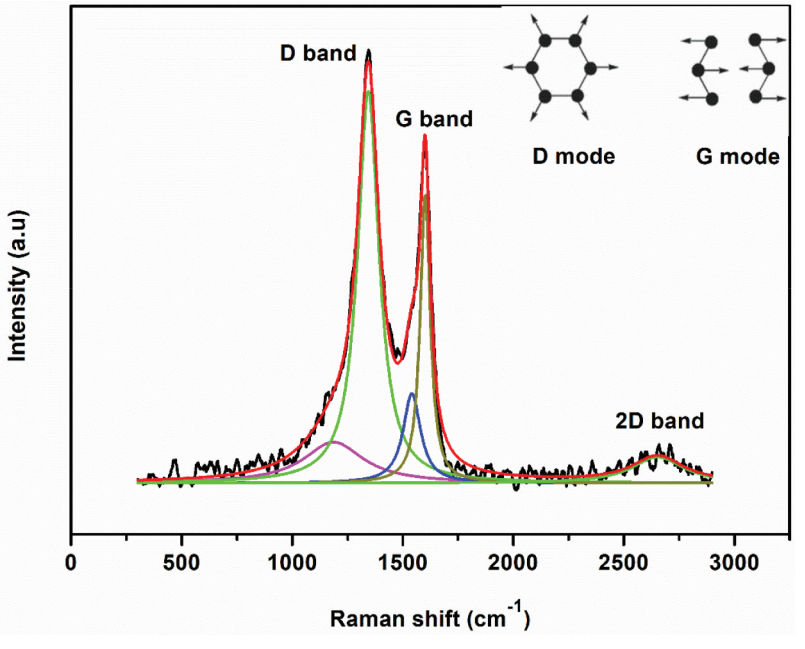

Figure 2. Raman spectrum of pinewood biochar.

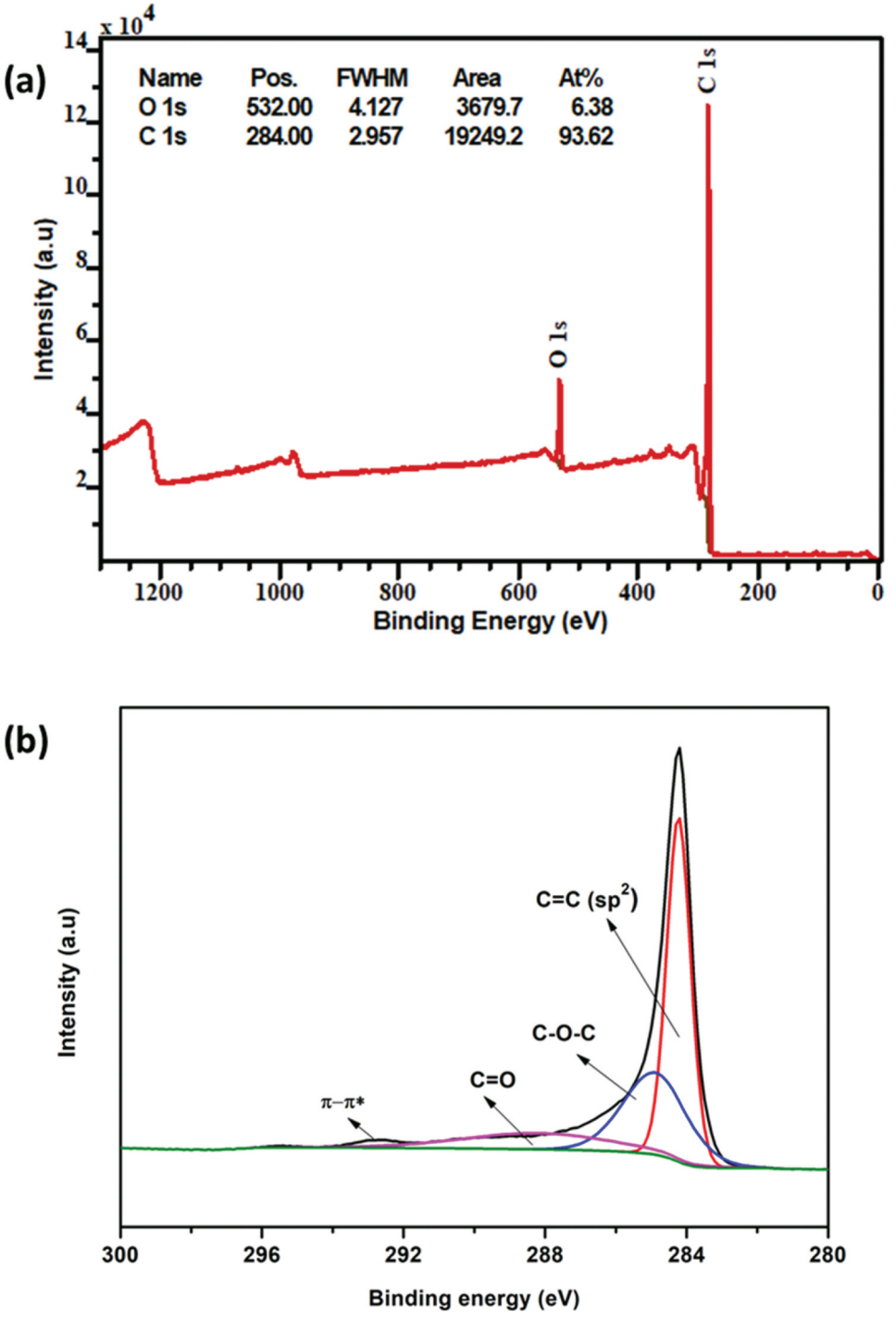

Figure 3. (a) XPS survey spectrum and (b) HR-XPS of pinewood biochar.

shown that the increase in $I_D/I_G$is an indicator of the increase in defect density of the carbon material [33].

A 2D broad peak is observed at ~2670cm^{-1}for pinewood biochar, Figure 2. The sizes and shapes of 2D peaks depend on the defect density associated with the carbon material. Ferreira *et al*. have shown that for Ar^+bombarded few-layer or single-layer graphene with high defect density has bumpy 2D peaks. This observation is due to defect-induced peaks and suppression of 2D peaks owing to the disruption of the hexagonal lattice [34]. Similarly, the defects significantly change the shape of 2D peaks in pinewood biochar. The Raman studies were conducted on biochar after size reduction, which would have affected the shape of the 2D peak. Here, defects could also arise from the high-temperature pyrolysis.

3.3. Elemental analysis and functional groups of biochar

The XPS survey spectrum of pinewood biochar, Figure 3(a), provides the percentage composition of elements present in the biochar. The major components of pinewood biochar are carbon (93.62 at%) and oxygen (6.38 at%). In order to determine the quantity of sp^2carbon, and to assess the percentage of various functional groups, an in-depth analysis of the high-resolution C1s of pinewood biochar was conducted. The high-resolution quantitative C1s spectrum reveals a peak at ~284eV, which is due to sp^2 hybridised carbon from graphitic cluster. From Figure 3(b), the percentage of sp^2 carbon can be calculated as ~69.60%. By resolving the core spectrum C1s gives a peak at ~286.7eV and at ~288eV which correspond to the epoxy group (~17.12%) and carbonyl group, respectively. These functional groups are mostly present on the edges or at the defects on the graphene layers. It must be noted that the percentage of sp^2carbon has considerably improved with high-temperature pyrolysis. The sp^2carbon content of biochar is responsible for its electrical conductivity. Therefore, an improvement in sp^2 carbon content leads to an improvement in electrical conductivity despite any defects associated with biochar. This highlights the importance of maximizing the production of sp^2 carbon during the pyrolysis process, as it can significantly impact the electrical properties of the material.

3.4. HR-TEM of pinewood biochar

Figure 4 shows the high-resolution transmission electron microscopy (HRTEM) of *p*-1200 with a fast Fourier Transform (FFT) in the inset. The selected area electron diffraction (SAED) is provided by the FFT, showing a hexagonal lattice with an average lattice spacing of ~0.24nm, Figure 5, which is close to the lattice spacing reported for graphitic crystal earlier [35]. In all HRTEM images, we can visualize the crystalline regions (darker regions with lattice fringes) and amorphous regions (lighter regions with no lattice fringes). Hence, HRTEM provides a visualization of graphitic clusters and their size, lattice spacing. The HRTEM can be used to understand the growth and evolution of graphitic structures in biochar with pyrolysis temperature.

Figure 5 shows the HRTEM image of *p*-1200 and lattice spacing. The average spacing between the atoms is ~0.24nm, which is comparable to the graphene lattice spacing. The

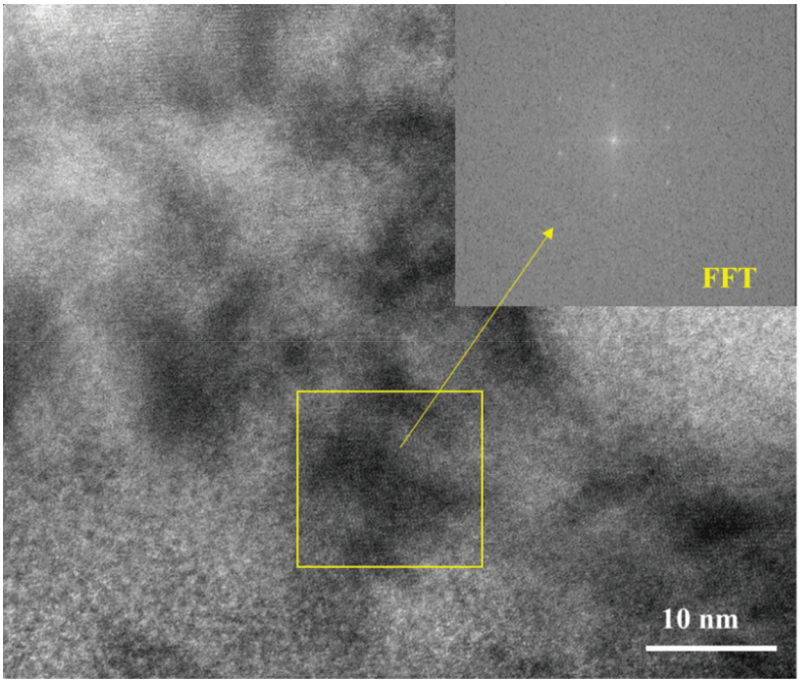

Figure 4. HRTEM image of biochar (*p*-1200) and the inset shows fast Fourier transform (FFT) from a selected area yellow square with Bragg spots.

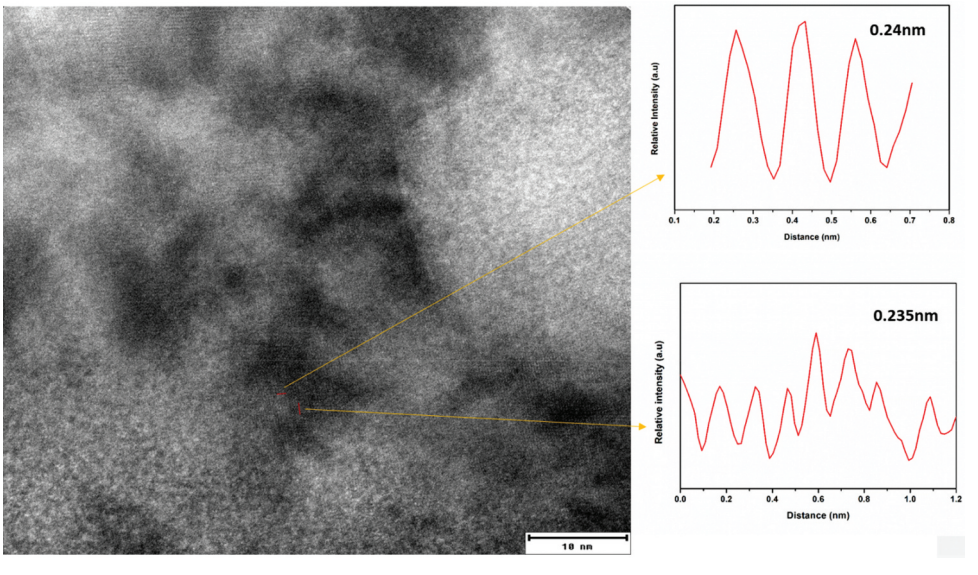

Figure 5. HRTEM of *p*-1200 and lattice spacing measured using imageJ.

HRTEM provides evidence of graphitic growth in the biochar at high-temperature pyrolysis.

3.5. Characterisations of polymer composites

3.5.1. Biochar polymer matrix interaction from tensile fractured surface

Figure 6 depicts the fractured surface of pinewood biochar PLA-based pinewood biochar polymer composites. The image reveals the separation of PLA and PBAT phases, resulting from the incompatibility of these two phases. Figures 6(a,b) show the tensile fracture surface of PLA (80/20) and PLA (79/20/1), respectively. The fiber-like structures seen in images are PBAT phases that have been deformed plastically during tensile testing; this is expected due to the ductile nature of PBAT. Moreover, the biochar particles are coated with the polymer, enhancing the polymer matrix interfacial interaction with biochar. However, an increase in biochar content gives rise to the emergence of bead structures. This structure comprises the PBAT phase dispersed in the PLA matrix. The main component of the composite is PLA, in which PBAT and biochar powder are dispersed.

3.5.2. Thermal properties of polymer composites

Figure 7 displays the heating curve of the PLA and PBAT blend, and PLA, PBAT and pinewood biochar composites, displaying two transitions in the DSC thermogram: cold crystallization exotherm and melting endotherm. The cold crystallization exotherm of the PLA (80/20) blend appeared at around 101.54, with the melting endotherm at 176.05.

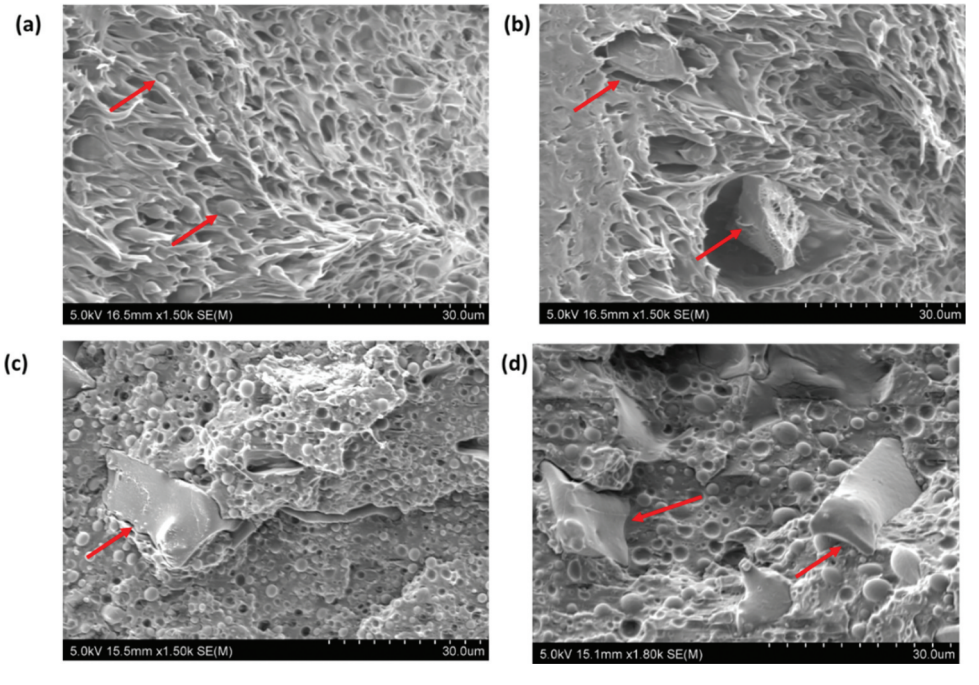

Figure 6. SEM images of (a) PLA (80/20), (b) PLA (79/20/1), (c) PLA (75/20/5) and (d) PLA (70/20/10) [red arrows in Figure 5(a) show PBAT phase, red arrows in Figure 3(b-d) represent pinewood biochar].

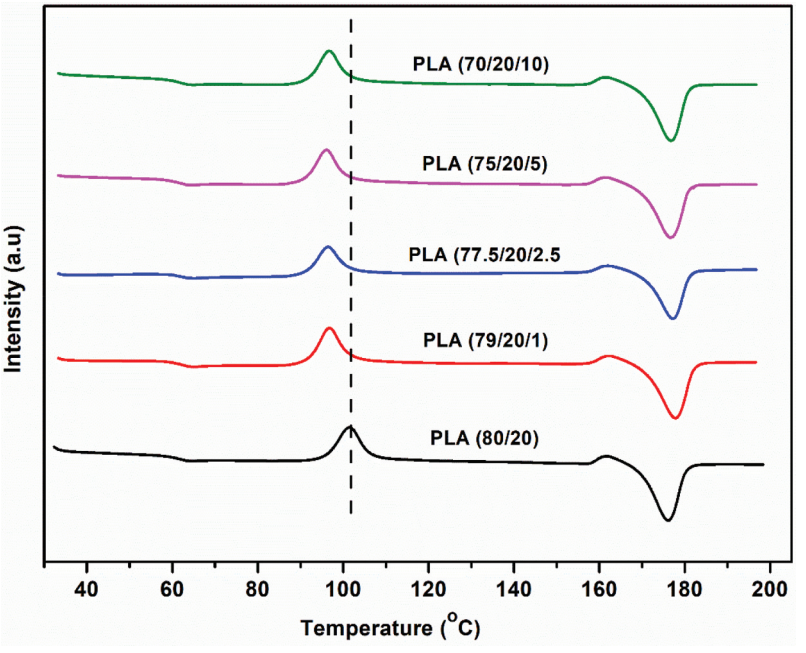

Figure 7. DSC analyses of PLA/PBAT20/BC composites.

Table 2. The percentage crystallization of PLA/PBAT composites.

Sample	T_c []	T_m[]	ΔH_{cc}[J/g]	ΔH_m[J/g]	X_c (%)
PLA (80/20)	101.5	176.1	17.4	34.3	22.5
PLA (79/20/1)	96.7	177.8	18.9	38.0	25.8
PLA (77.5/20/2.5)	96.5	177.2	15.4	36.5	29.0
PLA (75/205)	96.1	176.1	17.4	38.1	29.8
PLA (70/20/10)	96.7	176.6	18.5	40.9	34.1

Pinewood biochar addition to the polymer matrix shifted the cold crystallization temperatures of the composites towards the low-temperature region, which is due to the nucleation by the biochar particles. This improvement in crystallization improves the percentage crystallization of PLA in the composites, with the PLA (80/20) blend having 22.53% crystallization and PLA (70/20/10) composite with 10 wt% of biochar showing 34.14% (Table 2) of crystallization – an improvement of 51.53% with the addition of 10 wt % of pinewood biochar.

T_c -cold crystallization, T_m-melting temperature, ΔH_{cc}- enthalpy change (cold crystallization), ΔH_m-enthalpy change (melting), X_c- degree of crystallinity

3.5.3. Thermal degradation

Figure 8 shows the TGA and differential thermogravimetry (DTG) of the pinewood biochar PLA/PBAT blend and composites. The initiation of degradation in the PLA/PBAT blend appeared around ~347. Table 3 summarizes the initiation of degradation (T_5, the temperature at which 5 wt% of degradation occurs) and maximum thermal degradation (T_{max}) and char residue at 550. The TGA curve shows two weight losses; the initial weight

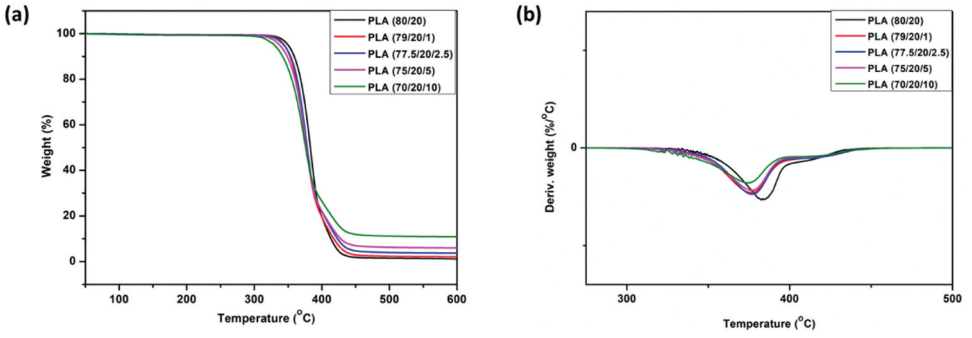

Figure 8. (a) TGA (b) DTG of PLA/PBAT pinewood biochar composites.

Table 3. Degradation onset (T_5), the maximum degradation temperature (T_{max}) and residual char (%) at 550.

Sample	$T_5()$	$T_{max}()$	Char residue at 550(%)
PLA (80/20)	347.0	382.9	1.4
PLA (79/20/1)	344.2	377.8	2.3
PLA (77.5/20/2.5)	343.8	377.2	3.8
PLA (75/20/5)	337.4	376.8	6.1
PLA (70/20/10)	329.6	373.7	11.0

loss corresponds to the PLA degradation, and the final weight loss appears between 400to 450, to PBAT. As expected, the biochar in the PLA/PBAT composites shows no degradation, and the percentage weight of char residue at 550 increases with biochar content, with the majority of the residue, being the thermally stable biochar particles.

The degradation initiated at a lower temperature for the biochar composites compared to the PLA and PBAT blend. The degradation temperature of the biochar composites lowered with an increase in pinewood biochar concentration, however it decreased with the PLA weight percentage. As the content of PLA decreases, the onset of degradation and maximum degradation temperature starts at lower temperatures (Table 3), indicating that the thermal stability of the PLA/PBAT blend is higher than that of the PLA/PBAT biochar composites.

3.5.4. Mechanical properties

For the application of biochar added PLA/PBAT composites for personal-protective-equipment (PPE), a combined mechanical and electrical conductivity in the antistatic region is essential. Figure 9 shows the mechanical properties of the PLA and PBAT blend and pinewood biochar incorporated PLA/PBAT composites. The addition of 1 wt% of biochar resulted in an improvement of the tensile strength of the PLA/PBAT blend by approximately 53.8%. However, further addition of biochar causes a decrease in tensile strength, reaching values to those of PLA/PBAT blend with biochar at 10 wt%. The increase in the tensile strength is due to the enhanced interfacial interaction of the biochar with the polymer matrix. Biochar particles can deviate some of the stress from the polymer matrix, preventing the generation of cracks [21]. Moreover, a low biochar concentration improves the miscibility between the PLA and PBAT phases and enhances their interfacial interactions. However, the agglomeration of biochar particles at high

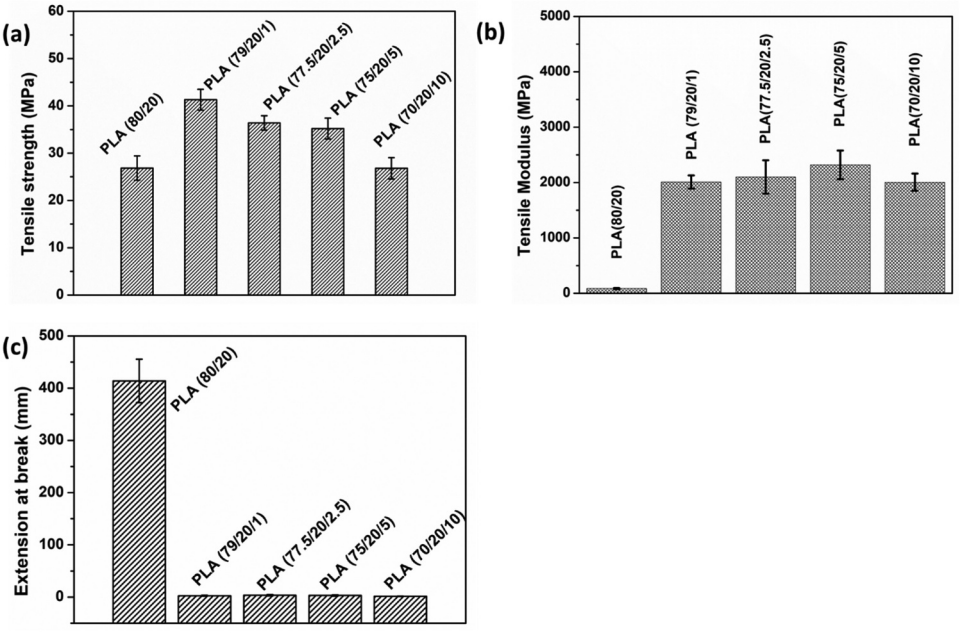

Figure 9. (a) tensile strength (b) tensile modulus (c) elongation at break of PLA/PBAT blend and composites.

concentrations leads to a decrease in tensile strength [36]. Similar behavior was observed in PLA/PBAT/CSB composites [25]. The incorporation of pinewood biochar into the PLA and PBAT blend has drastically reduced the elongation at break of the composites, making them more brittle [Figure 9(c)]. However, even with the addition of 1 wt% to the PLA/PBAT polymer matrix, there is an impressive 1581% improvement in the average tensile modulus of the composites, Figure 9(b).

3.5.5. Rheological analyses of PLA/PBAT composites

The melt rheology properties depend on factors such as phase morphology, the structure of the polymer chain, and filler–matrix interaction [37,38]. In order to understand both the microstructure and thermal properties of the polymer, it is necessary to examine the microstructure-process connection. The filler network formation can be demonstrated through the appearance of the plateau of the storage modulus curve at lower frequencies. Figure 10 and Figure 11 display changes in storage modulus (G'), loss modulus(G''), loss factor and viscosity of the blend and composites.

The angular frequency *AccessisdeniedAccessisdenied*verses storage moduli *AccessisdeniedAccessisdenied* of PLA/PBAT composites with different weight percentages of pinewood biochar are shown in Figure 10(a). It can be observed that the storage modulus of PLA/PBAT blend improved with the addition 1 wt% of biochar. The composite with 1 wt% of biochar content shows the highest storage modulus. First, there is a drastic increase in storage moduli with an increase in biochar content (maximum for 1 wt%), which then decreases with an increase in biochar content in the composites but has values above the PLA/PBAT blend. However, the

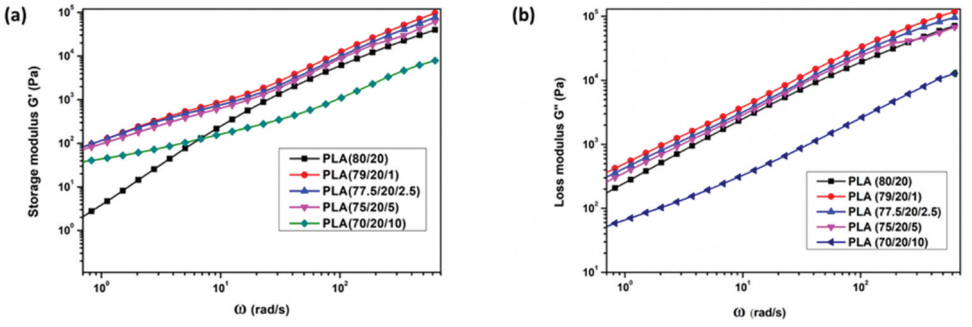

Figure 10. (a) Storage modulus and (b) loss modulus of PLA/PBAT biochar composites.

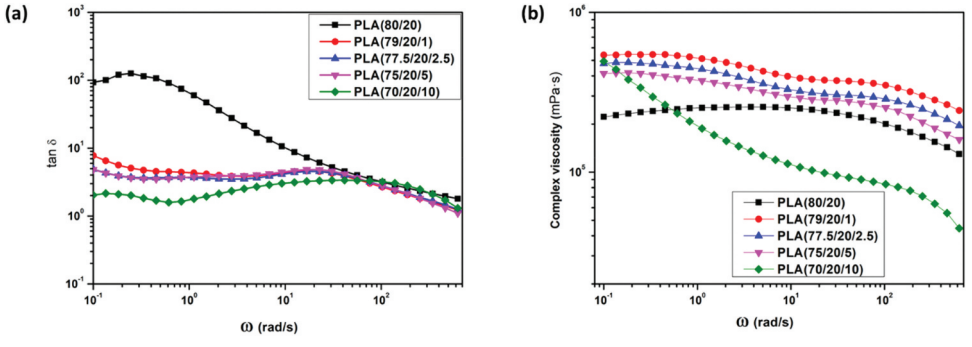

Figure 11. (a) thetan δ and (b) complex viscosity of PLA/PBAT biochar composites.

composite with 10 wt% of biochar shows a higher storage modulus than the PLA/PBAT blend at lower frequencies, but the storage modulus shows a lower value than that of the blend at higher frequencies. At low concentrations of biochar loading, biochar particle acts as a reinforcing agent and improves the rigidity of the composites; however, beyond 5 wt%, the storage modulus decreases due to the difficulty in maintaining the structural integrity of the composites. Moreover, the storage modulus could also be decreased due to the agglomeration of the filler particles at high biochar loading concentration (10 wt%), which could be a reasons for the lowering of storage modulus with high loading concentration biochar [39].

The plot of loss factor (tan δ) the ratio of loss modulus $(G^{''})$ and storage modulus $(G^{'})$) versus frequency data is shown in Figure 11. The melt viscosity of the composites with low loading of biochar shows behavior similar to that of the PLA/PBAT blend [39]. An increase in viscosity has been found for the composite with 1 wt% of biochar; however, viscosity decreases with an increase in biochar content, and when the biochar content reaches 10 wt%, the viscosity shows a drastic decrease with increasing frequency. The decrease in viscosity of the composite with high-concentration biochar could be due to the plasticizing effect of biochar particles. This effect could only be observed at high-loading concentrations of biochar; at low concentrations, biochar particles can occupy interfacial regions of the polymer chain, restricting the polymer chain motion.

Table 4. Surface resistivities of pinewood biochar pla-based composites.

Material	Surface resistivity (ohm/square) Mean± SD
PLA (80/20)	$1.58 \times 10^{13} \pm 0.09 \times 10^{13}$
PLA (79/20/1)	$4.72 \times 10^{12} \pm 0.23 \times 10^{12}$
PLA (77.5/20/2.5)	$2.67 \times 10^{12} \pm 0.18 \times 10^{12}$
PLA (75/20/5)	$1.24 \times 10^{12} \pm 0.16 \times 10^{12}$
PLA (70/20/10)	$4.86 \times 10^{10} \pm 0.25 \times 10^{10}$

3.5.6. Electrical conductivity values of the composites

Personal protective equipment (PPE) is often used in dangerous explosive atmospheres in industries like mines, petrochemicals and power stations. The most common reason for explosions in such an environment is the charges accumulated on PPE equipment. In order to prevent such accidents, it is crucial to use antistatic and electrostatic dissipative materials for PPE manufacturing [24]. Ideally, these materials should be eco-friendly, sustainable, biodegradable and possess antistatic properties. While considering environmental benefits and antistatic properties, using eco-friendly, sustainable and biodegradable antistatic material for PPE manufacturing is desirable. Electrically conductive biochar-reinforced PLA/PBAT composites would be suitable for such applications.

Table 4 shows the surface resistivity of the composite with different loading concentrations of pinewood biochar. The addition of 10 wt% of pinewood biochar decreased the surface resistivity of the composite by 3 orders of magnitude. The decrease in surface resistivity of biochar is due to the presence of sp^2 hybridized carbon. Adding 10 wt% of pinewood biochar to the polymer matrix does not drastically decrease the electrical resistivity of the composite; however, the surface resistivity of 10 wt% biochar composite show lower resistivity than previously reported values [24]. Moreover, the electrical conductivity of the composite with 10 wt% of biochar is suitable for antistatic material [9]. While compared to the previously studied 10 wt% coconut shell biochar PLA/PBAT composites, the electrical resistivity has increased by an order of magnitude [25].

3.5.7. Thermal conductivity values of PLA/PBAT biochar composites

Figure 12 shows the thermal conductivity of the pinewood biochar composites at three different temperatures (25, 35 and 45). The thermal conductivity of the PLA/PBAT matrix at25 is $0.178\mathrm{W/mK}$, and for composite with 10 wt% of biochar is $0.214\mathrm{W/(mK)}$. The thermal conductivity of the composites improved with the loading of biochar. At low concentrations of biochar, there is no appreciable change in thermal conductivity; however, there is $\sim 20.22\%$ improvement in the thermal conductivity of the composite with the addition of 10 wt% of biochar. The increased thermal conductivity of the composites with high concentrations of biochar is due to the interconnectedness of the biochar particles in the polymer matrix. The thermal carriers (phonons) can propagate through a least resistive path created by interconnected biochar particles in the polymer matrix [29].

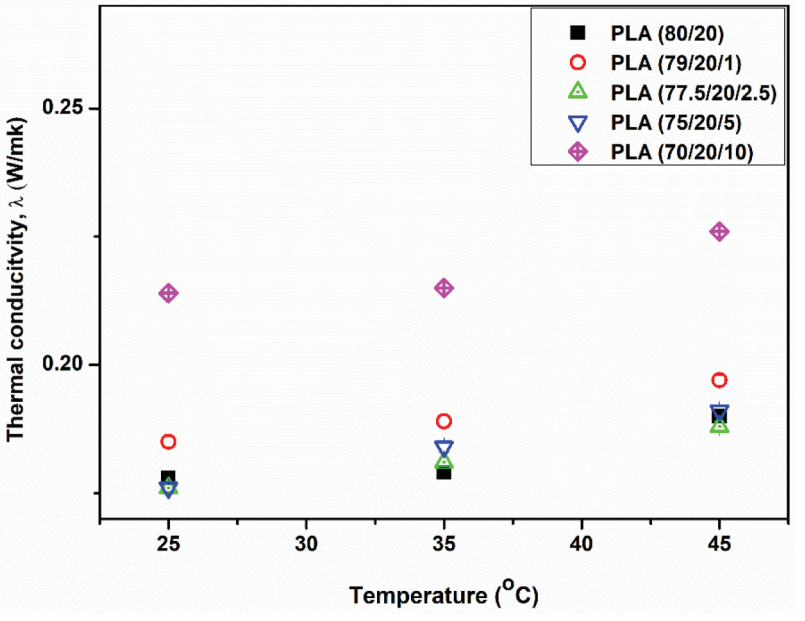

Figure 12. Thermal conductivity values of the PLA/PBAT composites.

4. Conclusions

Agricultural waste-derived pinewood biochar is a suitable conductive and reinforcing-filler material for PLA/PBAT polymer matrix. Pinewood biochar addition to PLA/PBAT improved the composites' mechanical and electrical properties. Electrically conductive pinewood biochar was produced through the pyrolysis of pinewood firewood. The biochar was characterized in depth using Raman spectroscopy and X-ray spectroscopy. The spectroscopic studies revealed that the amount of sp^2 carbon content improved with high-temperature pyrolysis. Raman studies showed that the biochar produced through pyrolysis had a high concentration of defect density.

The biochar was used to prepare PLA/PBAT biochar composites with different loading concentrations. The tensile strengths of the composites with 1 wt% of biochar have shown an improvement of ~53.81%, which is much higher than the previously reported values. The improvement in the tensile strength of the composite is due to a better interfacial interaction of the biochar particles with the polymer matrix. The thermal studies of PLA/PBAT composites show that the total crystallinity of the composites improves by increasing biochar concentration. Moreover, the decrease in cold crystallization of the composite is primarily due to the nucleating effect of biochar particles. The electrical studies have revealed that the surface resistivity of the composite with 10 wt% of biochar is reduced by 3 orders of magnitude when compared to that of the PLA and PBAT blend. The surface resistivity of 10 wt% biochar composite is found to be $4.86 \times 10^{10}\Omega/\text{sq}$ and is suitable for antistatic applications. The addition of biochar has improved the thermal conductivity of the composite due to the formation of the interconnected network within the

polymer matrix. Hence, pinewood biochar is an eco-friendly, sustainable, low-cost, electrically conductive PLA/PBAT polymer matrix filler. In addition, these composites are suitable for antistatic applications.

Disclosure statement

No potential conflict of interest was reported by the author(s).

Funding

The work was supported by the Ministry for Business, Innovation and Employment (MBIE).

References

[1] Jachowicz M. Electrostatic properties of selected personal protective equipment regarding explosion hazard. J Sustain Min. 2013;12(1):27–33. doi: 10.7424/jsm130106
[2] Kathirgamanathan P, Toohey MJ, Haase J, et al. Measurements of incendivity of electrostatic discharges from textiles used in personal protective clothing. J Electrostat. 2000;49(1):51–70. doi: 10.1016/S0304-3886(00)00003-6
[3] Yadav R, Tirumali M, Wang X, et al. Polymer composite for antistatic application in aerospace. Def Technol. 2020;16(1):107–118. doi: 10.1016/j.dt.2019.04.008
[4] de Souza Vieira L, dos Anjos EGR, Verginio GEA, et al. Carbon-based materials as antistatic agents for the production of antistatic packaging: a review. J Mater Sci: Mater Electron. 2021;32(4):3929–3947. doi: 10.1007/s10854-020-05178-6
[5] George J, Poulose AM, Chandran A, et al. Influence of plasticizer on the dielectric properties of polypropylene/carbon black composites. In: Materials Today: Proceedings, Auckland, New Zealand; 2023.
[6] Zhou S, Xu J, Yang Q-H, et al. Experiments and modeling of thermal conductivity of flake graphite/polymer composites affected by adding carbon-based nano-fillers. Carbon. 2013;57:452–459. doi: 10.1016/j.carbon.2013.02.018
[7] Ansari S, Giannelis EP. Functionalized graphene sheet—Poly(vinylidene fluoride) conductive nanocomposites. J Polym Sci Part B: Polym Phys. 2009;47(9):888–897. doi: 10.1002/polb.21695
[8] Othman NH, Che Ismail M, Mustapha M, et al. Graphene-based polymer nanocomposites as barrier coatings for corrosion protection. Prog Org Coat. 2019;135:82–99. doi: 10.1016/j.porgcoat.2019.05.030
[9] Choi H-J, Kim MS, Ahn D, et al. Electrical percolation threshold of carbon black in a polymer matrix and its application to antistatic fibre. Sci Rep. 2019;9(1):1–12. doi: 10.1038/s41598-019-42495-1
[10] Fan Y, Fowler GD, Zhao M. The past, present and future of carbon black as a rubber reinforcing filler – a review. J Cleaner Prod. 2020;247:119115. doi: 10.1016/j.jclepro.2019.119115
[11] Snowdon MR, Mohanty AK, Misra M. A study of carbonized lignin as an alternative to carbon black. ACS Sustain Chem & Eng. 2014;2(5):1257–1263. doi: 10.1021/sc500086v
[12] Giorcelli M, Savi P, Khan A, et al. Analysis of biochar with different pyrolysis temperatures used as filler in epoxy resin composites. Biomass Bioenergy. 2019;122:466–471. doi: 10.1016/j.biombioe.2019.01.007
[13] Tharmaratnam T, Premachandra J. Investigation on the use of coconut shell powder replacing carbon black as filler in natural rubber. Tech Session-Sci Technol. 2015:44.
[14] Gabhi RS, Kirk DW, Jia CQ. Preliminary investigation of electrical conductivity of monolithic biochar. Carbon. 2017;116:435–442. doi: 10.1016/j.carbon.2017.01.069

[15] Gabhi R, Basile L, Kirk DW, et al. Electrical conductivity of wood biochar monoliths and its dependence on pyrolysis temperature. Biochar. 2020;2(3):369–378. doi: 10.1007/s42773-020-00056-0
[16] Liu Z, Fan T, Zhang D. Synthesis of biomorphous nickel oxide from a Pinewood template and investigation on a hierarchical porous structure. J Am Ceramic Soc. 2006;89(2):662–665. doi: 10.1111/j.1551-2916.2005.00741.x
[17] Cotana F, Cavalaglio G, Gelosia M, et al. Production of bioethanol in a second generation prototype from pine wood chips. Energy Procedia. 2014;45:42–51. doi: 10.1016/j.egypro.2014.01.006
[18] Brown S. Greenhouse gas accounting for landfill diversion of food scraps and yard waste. Compost Sci & Util. 2016;24(1):11–19. doi: 10.1080/1065657X.2015.1026005
[19] Thines K, Abdullah EC, Mubarak NM, et al. Synthesis of magnetic biochar from agricultural waste biomass to enhancing route for waste water and polymer application: a review. Renewable Sustain Energy Rev. 2017;67:257–276. doi: 10.1016/j.rser.2016.09.057
[20] Idrees M, Jeelani S, Rangari V. Three-dimensional-printed sustainable biochar-recycled PET composites. ACS Sustain Chem & Eng. 2018;6(11):13940–13948. doi: 10.1021/acssuschemeng.8b02283
[21] Giorcelli M, Khan A, Pugno NM, et al. Biochar as a cheap and environmental friendly filler able to improve polymer mechanical properties. Biomass Bioenergy. 2019;120:219–223. doi: 10.1016/j.biombioe.2018.11.036
[22] Liu W-J, Jiang H, Yu H-Q. Emerging applications of biochar-based materials for energy storage and conversion. Energy & Environ Sci. 2019;12(6):1751–1779. doi: 10.1039/C9EE00206E
[23] Brassard P, Godbout S, Lévesque V, et al. Biochar for soil amendment, in Char and carbon materials derived from biomass. Canada: Elsevier; 2019. p.109–146.
[24] Musioł M, Rydz J, Janeczek H, et al. (Bio)degradable biochar composites – studies on degradation and electrostatic properties. Mater Sci Eng: B. 2022;275:115515. doi: 10.1016/j.mseb.2021.115515
[25] George J, Jung D, Bhattacharyya D. Improvement of electrical and mechanical properties of PLA/PBAT composites using coconut shell biochar for antistatic applications. Appl Sci. 2023;13(2):902. doi: 10.3390/app13020902
[26] Benwood C, Anstey A, Andrzejewski J, et al. Improving the impact strength and heat resistance of 3D printed models: structure, property, and processing correlationships during fused deposition modeling (FDM) of poly (lactic acid). ACS Omega. 2018;3(4):4400–4411. doi: 10.1021/acsomega.8b00129
[27] Wootthikanokkhan J, Cheachun T, Sombatsompop N, et al. Crystallization and thermomechanical properties of PLA composites: effects of additive types and heat treatment. J Appl Polym Sci. 2013;129(1):215–223. doi: 10.1002/app.38715
[28] Zhou S-Y, Huang H-D, Ji X, et al. Super-robust polylactide barrier films by building densely oriented lamellae incorporated with ductile in situ nanofibrils of Poly(butylene adipate-co-terephthalate). ACS Appl Mater & Interface. 2016;8(12):8096–8109. doi: 10.1021/acsami.6b00451
[29] Bleija M, Platnieks O, Macutkevič J, et al. Poly(Butylene Succinate) hybrid multi-walled carbon nanotube/iron oxide nanocomposites: electromagnetic shielding and thermal properties. Polymers. 2023;15(3):515. doi: 10.3390/polym15030515
[30] Ferrari A, Robertson J. Origin of the 1 1 5 0– cm– 1 raman mode in nanocrystalline diamond. Phys Rev B. 2001;63(12):121405. doi: 10.1103/PhysRevB.63.121405
[31] Kaniyoor A, Ramaprabhu S. A Raman spectroscopic investigation of graphite oxide derived graphene. AIP Adv. 2012;2(3):032183. doi: 10.1063/1.4756995
[32] Maslova OA, Ammar MR, Guimbretière G, et al. Determination of crystallite size in polished graphitized carbon by Raman spectroscopy. Phys Rev B. 2012;86(13):134205. doi: 10.1103/PhysRevB.86.134205
[33] Xing T, Li LH, Hou L, et al. Disorder in ball-milled graphite revealed by Raman spectroscopy. Carbon. 2013;57:515–519. doi: 10.1016/j.carbon.2013.02.029

[34] Martins Ferreira EH, Moutinho MVO, Stavale F, et al. Evolution of the Raman spectra from single-, few-, and many-layer graphene with increasing disorder. Phys Rev B. 2010;82 (12):125429. doi: 10.1103/PhysRevB.82.125429
[35] Cong C, Li K, Zhang XX, et al. Visualization of arrangements of carbon atoms in graphene layers by Raman mapping and atomic-resolution TEM. Sci Rep. 2013;3(1):1195. doi: 10.1038/srep01195
[36] Poulose AM, Elnour AY, Anis A, et al. Date palm biochar-polymer composites: an investigation of electrical, mechanical, thermal and rheological characteristics. Sci Total Environ. 2018;619:311–318. doi: 10.1016/j.scitotenv.2017.11.076
[37] Wu S. Formation of dispersed phase in incompatible polymer blends: interfacial and rheological effects. Polym Eng & Sci. 1987;27(5):335–343. doi: 10.1002/pen.760270506
[38] Wu F, Zhang S, Chen Z, et al. Interfacial relaxation mechanisms in polymer nanocomposites through the rheological study on polymer/grafted nanoparticles. Polymer. 2016;90:264–275. doi: 10.1016/j.polymer.2016.03.034
[39] Nakayama D, Wu F, Mohanty AK, et al. Biodegradable composites developed from PBAT/PLA binary blends and silk powder: compatibilization and performance evaluation. ACS Omega. 2018;3(10):12412–12421. doi: 10.1021/acsomega.8b00823